Supplementary Information

3D-Printable, Highly Conductive Hybrid Composites Employing Chemically-Reinforced, Complex Dimensional Fillers and Thermoplastic Triblock Copolymers

Yejin Jo,[a,‡] Ju Young Kim,[a,b,‡] So-Yun Kim,[c,‡] Yeong-Hui Seo,[d] Kwang-Suk Jang,[e] Su Yeon Lee,[a] Sungmook Jung,[a] Beyong-Hwan Ryu,[a] Hyun-Suk Kim,[b] Jang-Ung Park,[c,*] Youngmin Choi,[a,*] Sunho Jeong[a,*]

[a]Division of Advanced Materials, Korea Research Institute of Chemical Technology (KRICT), 19 Sinseongno, Yuseong-gu, Daejeon 305-600, Korea. E-mail: youngmin@krict.re.kr; sjeong@krict.re.kr

[b]Department of Materials Science and Engineering, College of Engineering, Chungnam National University, 99 Daehak-ro, Yuseong-gu, Daejeon 305-764, Korea.

[c]School of Materials Science and Engineering, Wearable Electronics Research Group, Smart Sensor Research Center, Ulsan National Institute of Science and Technology (UNIST), Ulsan 689-798, Korea. E-mail: jangung@unist.ac.kr

[d]Department of Materials Science and Engineering, University of Illinois at Urbana-Champaign, Urbana, IL, USA

[e]Department of Chemical Engineering, Hankyong National University, 327 Jungang-ro,

Anseong 17579, Republic of Korea

‡Y. Jo, J. Y. Kim, S.-Y. Kim contributed equally.

Fabrication of Wireless Power Transmission Modules. The wireless power transmission modules were composed of a receiving antenna, a rectifying circuit and an OLED. To prepare the receiving antennas on the non-planar substrates, we first prepared SU8 structures by photolithographic patterning of SU8 (SU-8 3050, MicroChem Corp.) on PET substrates. The cylindrical (diameter = 350 μm and thickness = 50 μm) and rectangular structures with grooves (area = 80 x 80 μm^2 and thickness = 50 μm) were periodically arranged with a center-to-center distance of 4350 μm and 120 μm, respectively. After that, the hybrid composite paste was printed onto a planar/non-planar substrate that had 6 helical turns as an inner coil and a single turn as an outer coil with a 500 ± 50 μm line width. The rectifier was composed of a commercial silicon diode and a capacitor that were connected in a series, and an OLED was arranged in parallel to the circuit. The OLED was manufactured by spin-coating of 50 nm-thick poly(3,4-ethylenedioxythiophene):poly(styrenesulfonate) (AI4083, Clevios) and a 100 nm-thick emitting layer (PDY-132, Merck) on a ITO coated glass substrate. After that, LiF (1 nm)/Al (100 nm) was thermally evaporated for the cathode electrode. In order to harvest the radio frequency power, sine waves (frequency = 78 MHz and 80 MHz and amplitude = -13 dBm) were generated using a signal generator (N5183A MXG Analog Signal Generator, Agilent) and were amplified as much as 55 dB by a power amplifier (A-300RF power amplifier, Electronic Navigation Industries). This amplified AC signal was fed to a transmitting antenna, which was designed to have a single loop coil. After that, the AC signal was transmitted to the receiving antennas by inductive coupling. Finally, the wirelessly received AC signal with over 11 V_{rms} was converted to a DC signal through the rectifying circuit in order to operate the OLED.

Table S1. Elemental analysis results of pristine MWCNTs and NH_2-MWCNTs

MWCNT	C (%)	H (%)	N (%)	S (%)
pristine MWCNT	97.0	-	-	-
NH_2-MWCNT	89.7	1.0	2.7	-

Table S2. Conductivities of pristine MWCNT(50 wt%)/PVDF(50 wt%) and NH_2-MWCNT (50 wt%)/PVDF(50 wt%) composite films

Filler	Film thickness (μm)	Conductivity (S/cm)
Pristine MWCNT	11.2	9.9
NH_2-MWNCT	6.9	11.9

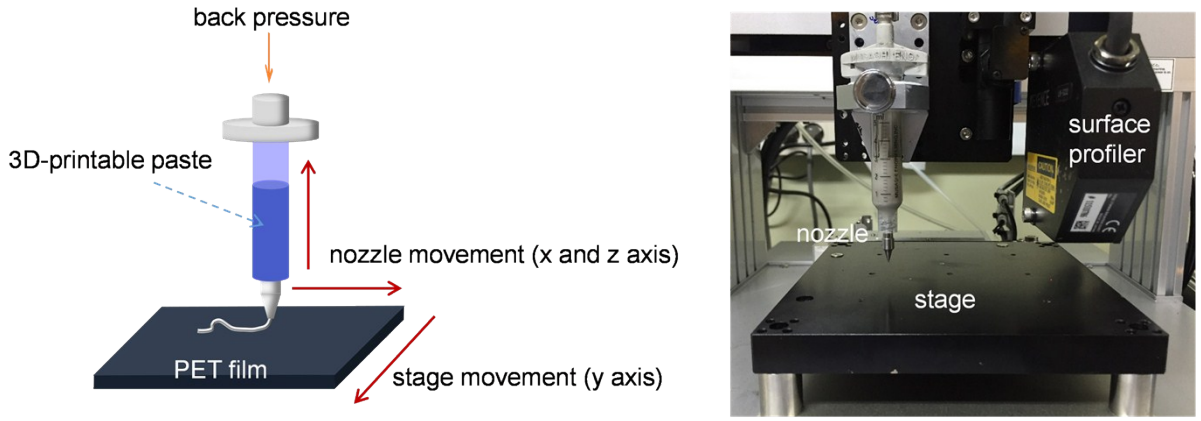

Figure S1. The schematic and picture of printing machine used in this study.

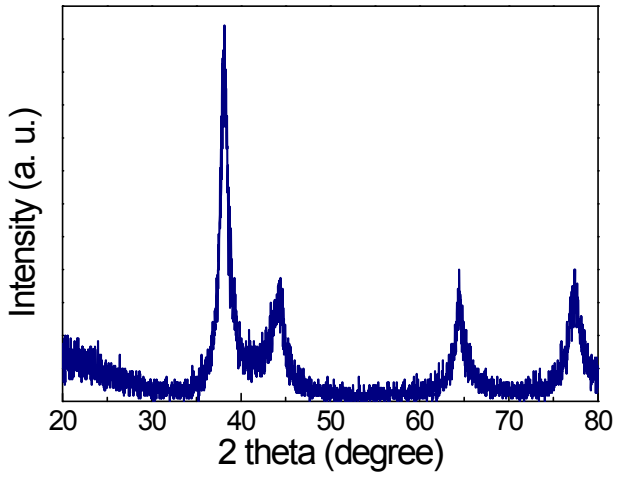

Figure S2. XRD result for PAA-capped silver nanoparticles.

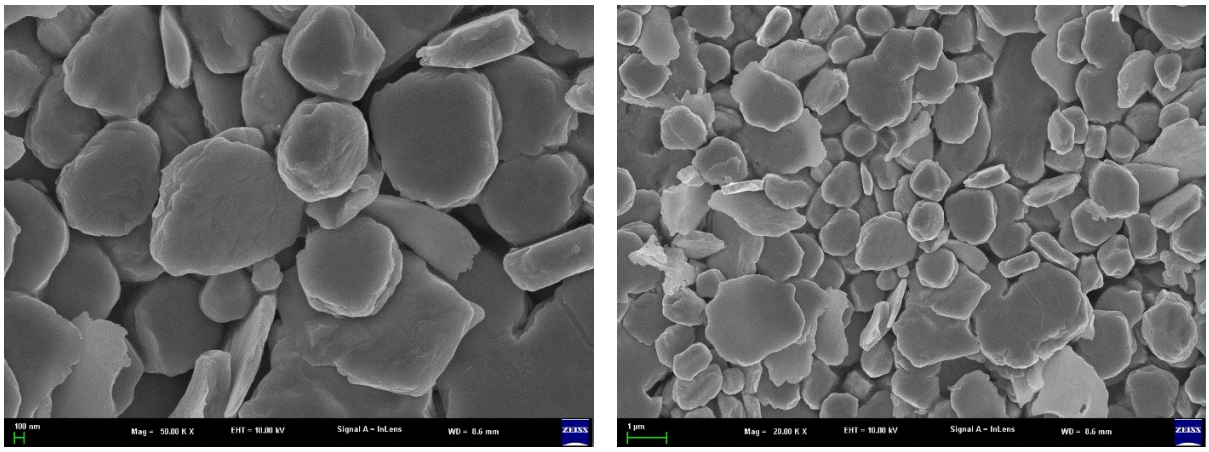

Figure S3. SEM image for Ag flakes used in this study.

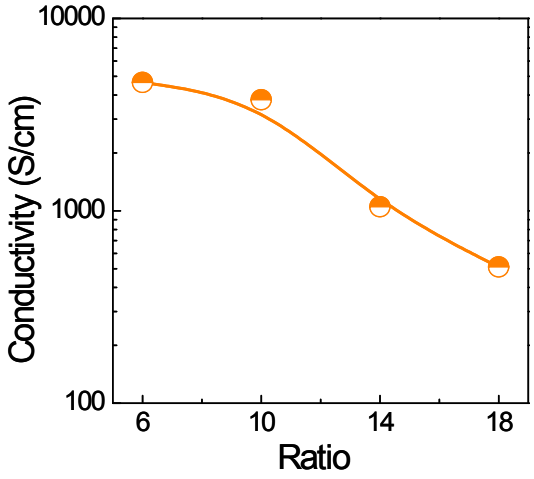

Figure S4. The conductivity evolution of composite materials, composed of NH_2-MWCNT, PAA-Ag NP, Ag flake and SIS triblock copolymer, depending on the ratio of Ag flake to the PAA-Ag NP/NH_2-MWCNT hybrid. The filler composition was 88 wt% in dried films and the solvent composition was 40 wt% in the paste

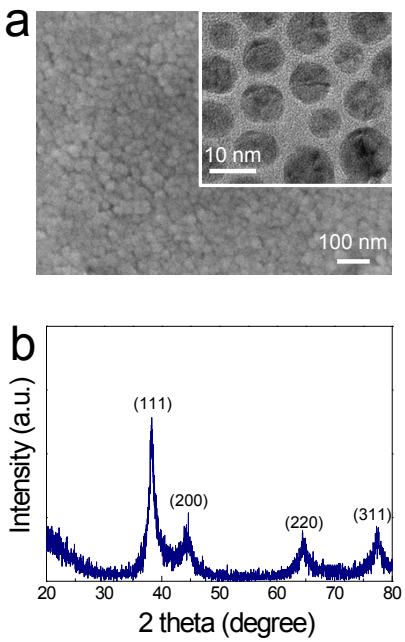

Figure S5. (a) SEM and TEM (inset) images and (b) XRD results for oleic acid-capped silver nanoparticles.

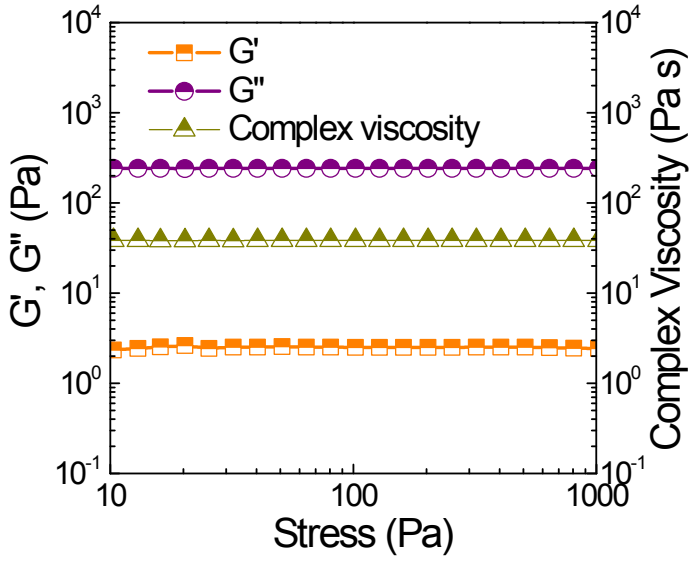

Figure S6. The rheological properties of polymer solution including SIS without fillers. The concentration of polymer was 32 wt%.

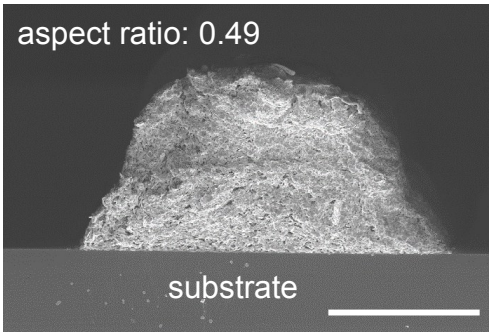

Figure S7. The cross-sectional image for the pattern printed using a hybrid composite material. The filler composition was 94 wt% in a dried film, the weight ratio of Ag flakes to the PAA-Ag NP/NH_2-MWCNT hybrid was 14, and the solvent composition was 16 wt% in the paste. The scale bar is 100 μm.

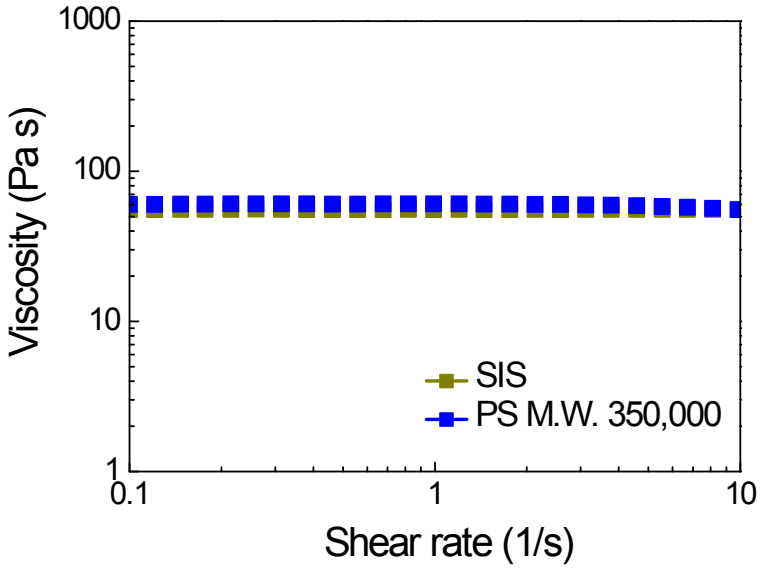

Figure S8. The viscosities of polymer solutions comprising either dichlorobenzene and SIS, or dichlorobenzene and PS with a molecular weight of 350,000. The concentration of polymers was 32 wt%.

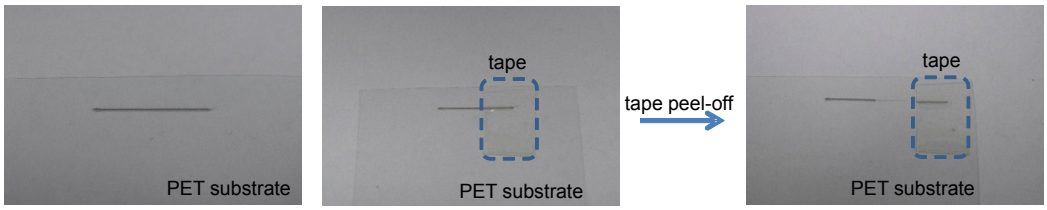

Figure S9. The adhesion test results for line patterns printed using composite paste employing PS with a molecular weight of 350,000. The filler composition was 94 wt% in a dried film, the weight ratio of Ag flake to the PAA-Ag NP/NH_2-MWCNT hybrid was 14, and the solvent composition was 16 wt% in the paste.

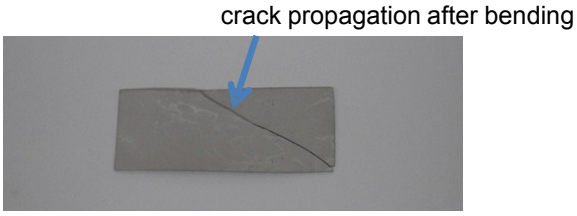

Figure S10. The photograph for the film, prepared using composite paste employing PS with a molecular weight of 350,000, after once simple bending test. The filler composition was 94 wt% in a dried film, the weight ratio of Ag flake to the PAA-Ag NP/NH_2-MWCNT hybrid was 14, and the solvent composition was 40 wt% in the paste.

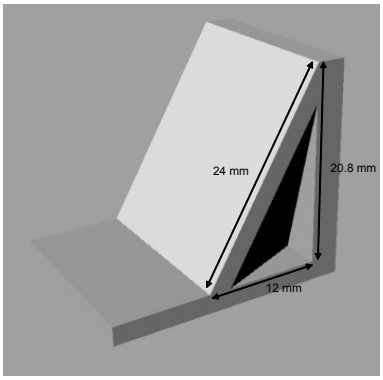

Figure S11.The dimension of the SLA-printed structure.

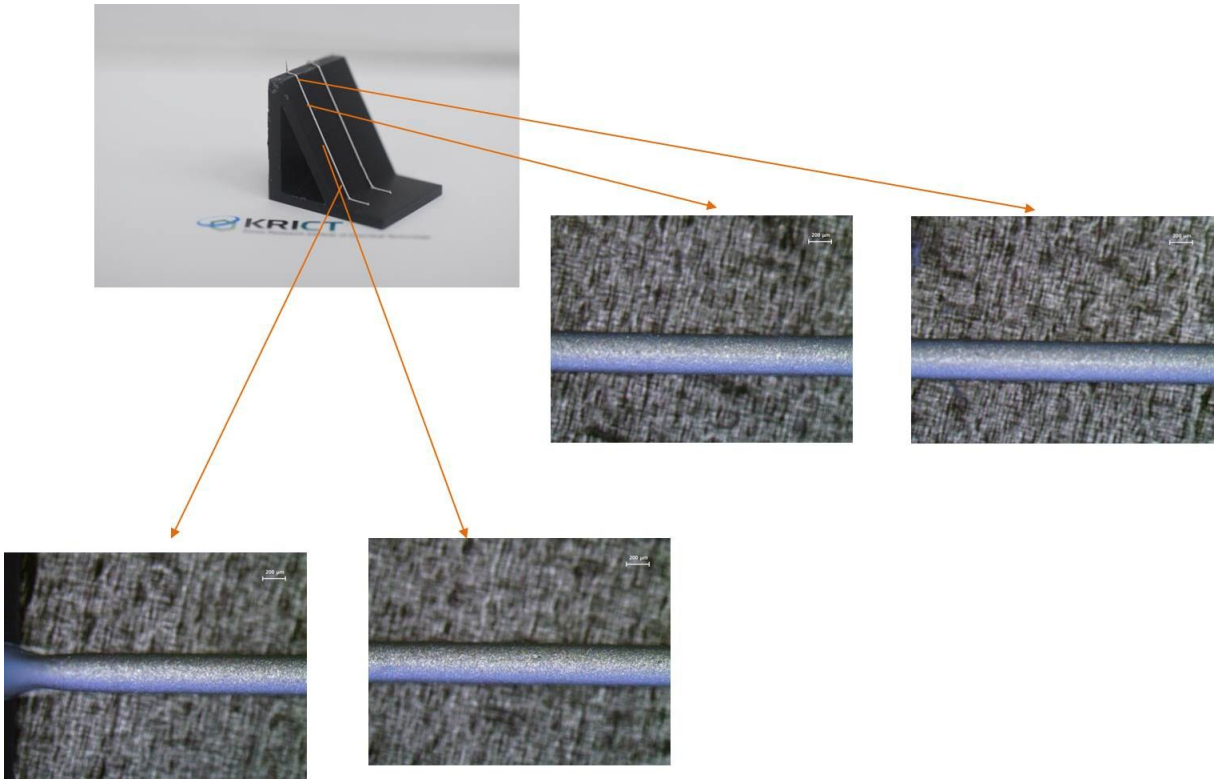

Figure S12. The optical microscopy images for line pattern printed on the SLA-printed structure with a slope of 60^{o}.

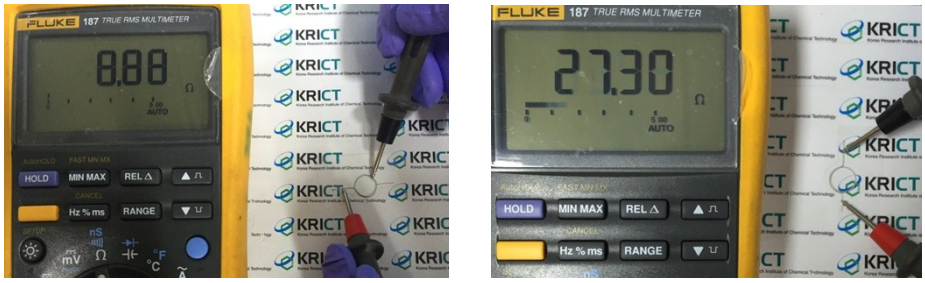

Figure S13. Photographs showing the electrical current flow between the side line and the top layer, and between both side lines.

Figure S14. Photographs showing the "repairing" process for a broken electrical component by a simple dispensing of hybrid composite paste.

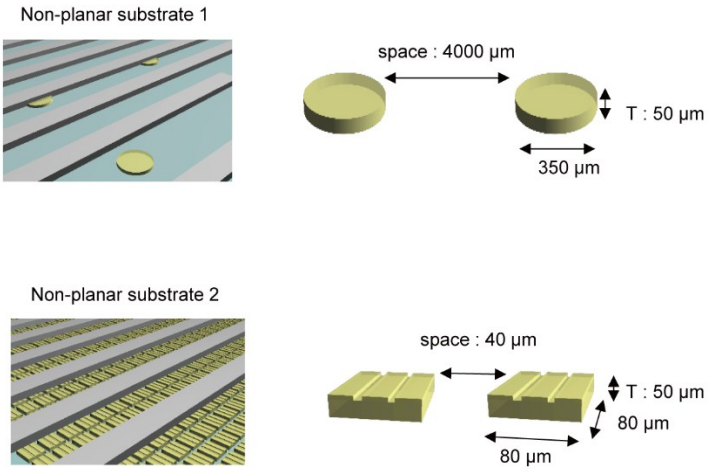

Figure S15. Schematic illustration showing the design of the SU-8 structures for fabrication of the non-planar substrates on PET films.

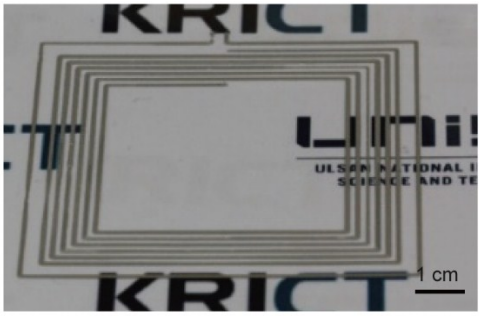

Figure S16. Photograph of the printed antenna on the planar PET substrate.

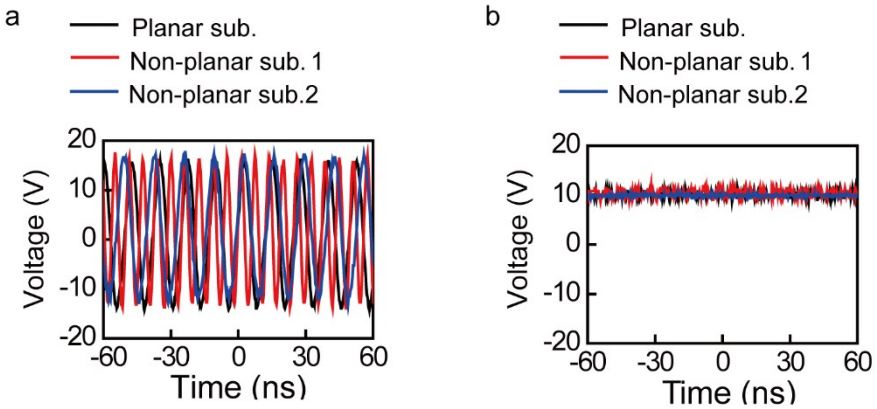

Figure S17. (a) The measured sinusoidal curves of transient voltages wirelessly transmitted to three different types of antennas, and (b) their rectified DC signals.

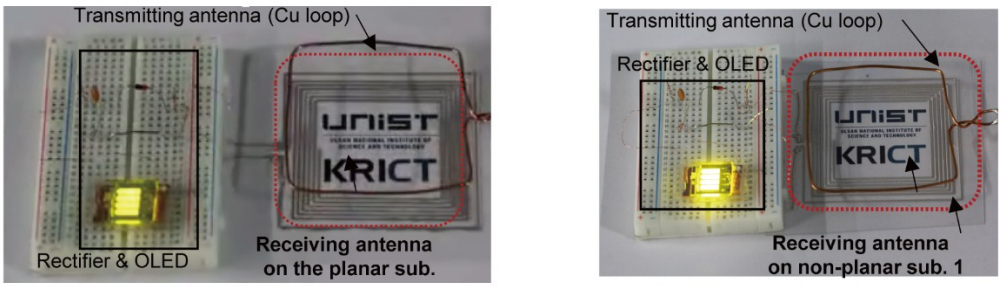

Figure S18. Wireless operation of the OLEDs using the antennas printed on the planar substrate and non-planar substrate 1.

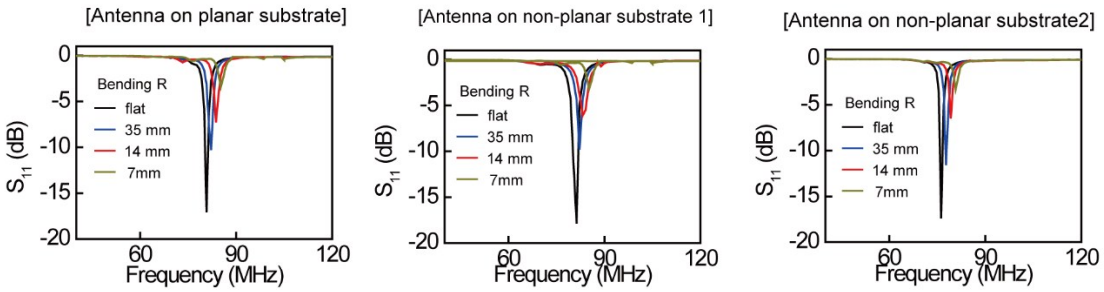

Figure S19. The frequency response of reflection coefficient (S_{11}) along with the mechanical bending by varying the radius curvature of the antennas printed on three types of substrates.

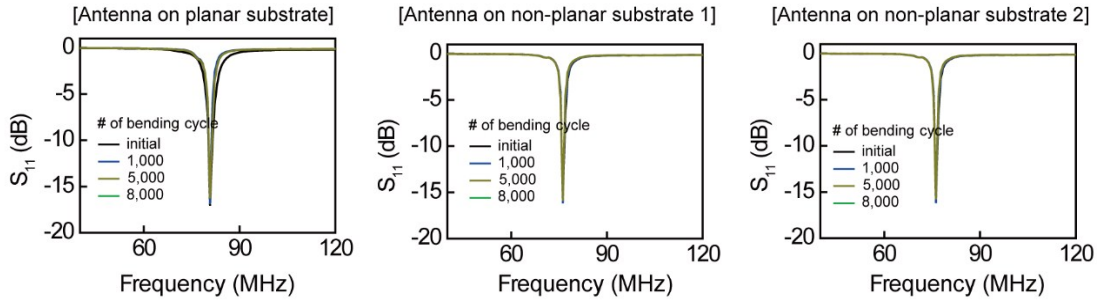

Figure S20. The frequency response of the reflection coefficient (S_{11}) along with the bending cycle (R = 7 mm) of the antennas printed on three types of substrates.

Movie S1. Motion picture showing the printing process using highly viscous composite paste.

Movie S2. Wireless power transmission module using an antenna on a planar substrate .

Movie S3. Wireless power transmission module using an antenna on a non-planar substrate 1.

Movie S4. Wireless power transmission module using an antenna on a non-planar substrate 2.